Nuclear Inst. and Methods in Physics Research, A 915 (2019) 102–109

Contents lists available at ScienceDirect

Nuclear Inst. and Methods in Physics Research, A

journal homepage: www.elsevier.com/locate/nima

Numerical evaluation of fast-sensitive microstructured semiconductor neutron detectors for TREAT hodoscope

Wenkai Fu, Ryan G. Fronk, Douglas S. McGregor, Jeremy A. Roberts *

Department of Mechanical and Nuclear Engineering, Kansas State University, Manhattan, KS 66506, USA

ARTICLE INFO

Keywords:
TREAT hodoscope
MSND
Fast neutron detector
Geant4

ABSTRACT

Presented is the numerical study of fast-sensitive, actinide and hydrogenous microstructured semiconductor neutron detectors (MSNDs) for the hodoscope at the Transient REActor Test facility (TREAT) using Geant4 and MCNP6. Neutron converters considered were ^{237}Np, ^{235}U, natural uranium, and ^{232}Th for actinide MSNDs and paraffin wax for hydrogenous MSNDs (H-MSNDs). Paraffin wax was found to have a larger fission-spectrum-weighted macroscopic cross section (0.32 cm $^{-1}$) than the actinide materials (the best being 0.067 cm $^{-1}$ for ^{237}Np). However, actinide reactants were found to allow higher lower-level discriminator (LLD) settings due to the large energy of fission fragments. Actinide MSNDs filled with ^{235}U, natural uranium, and ^{232}Th were evaluated in Geant4 using the fission fragment generator. With the LLD set to 5 MeV, the intrinsic neutron-detection efficiency of the ^{235}U-filled MSNDs was 1.2% for a 2-cm device length and saturated at 2.6% for lengths beyond 14 cm, where 20-μm trench and 10-μm wall widths were assumed. The deposited energy in ^{235}U predicted by Geant4 differed from the MCNP6-predicted value by about −0.7%. With the LLD set to 300 keV, Geant4 and MCNP6 predicted an efficiency of about 10% for a 2-cm long H-MSND with 20-μm trench and 10-μm wall widths and an efficiency of about 26% for a detector length of 20 cm. For a LLD set to achieve a signal-to-noise (S/N) ratio of 100 when including gamma-ray noise, the best-case, Geant4-predicted efficiencies were 2.5% and 9.6% for 2-cm and 20-cm long devices with 60-μm trench and 40-μm wall widths.

1. Introduction

Safety is a major concern in the peaceful use of nuclear technology, especially after the Fukushima nuclear accident. With increased interest in accident tolerant fuels, the TREAT facility at Idaho National Laboratory (INL), which enables testing fuel samples under simulated accident conditions, was restarted in late 2017 after two decades of no operation [1].

Shown in Fig. 1 is a schematic of the TREAT facility. A major component of the facility is the hodoscope, which consists of a steel collimator, a fast-neutron detector array, and the associated signal processing and data management subsystems [3]. The TREAT core can generate transient neutron fluxes up to 10^{17} cm^{-2}s^{-1} [4] to simulate accident conditions at the test section. The test section is targeted by the steel collimator, which connects the inner and the outer core volumes. During pulsing of a sample, fission neutrons born in the sample travel through different channels in the collimator and arrive at the detectors connected to the channels individually. The count rate of each detector forms a pixel of an image, thereby, revealing the fuel motion in the sample [3].

The hodoscope radiation consists of the collimated fast neutrons (signal) and the gamma rays. The gamma rays originate from several sources [3]. Prompt fission gamma rays arrive at the detectors through the collimator with the neutrons. These gamma rays may contribute to the identification of the fuel motion. Neutron-activation gamma rays generated in the steel collimator are identified as major sources of noise. The intensity of these capture gammas has been estimated to be approximately 9 per fast neutron [3]. Scattered gamma rays are also produced by Compton scattering, the photoelectric effect, and pair production [5].

Hornyak button fast-neutron detectors were used in the original hodoscope [3]. The detectors exhibited neutron-detection efficiencies of about 0.4% with a gamma-ray sensitivity of about one count per 10^8 incident gamma rays [3]. However, in the hodoscope, the detector suffered from strong gamma-induced Cherenkov noise. To reject such noise, a specialized pulse-shaping technique and lead filters were used [3]. These treatments, though successful, complicated the detection system.

Several Hornyak-button alternatives are under investigation at Kansas State University. Design of such alternatives aims for neutron-detection efficiencies larger than 1% at LLD settings that sufficiently reject the neutron-activation gamma rays in the hodoscope environment. To meet such requirements, fast-sensitive actinide and hydrogenous microstructured semiconductor neutron detectors (MSNDs) were

* Corresponding author.
E-mail address: jaroberts@k-state.edu (J.A. Roberts).

https://doi.org/10.1016/j.nima.2018.09.080
Received 16 May 2018; Received in revised form 11 September 2018; Accepted 17 September 2018
Available online 27 September 2018

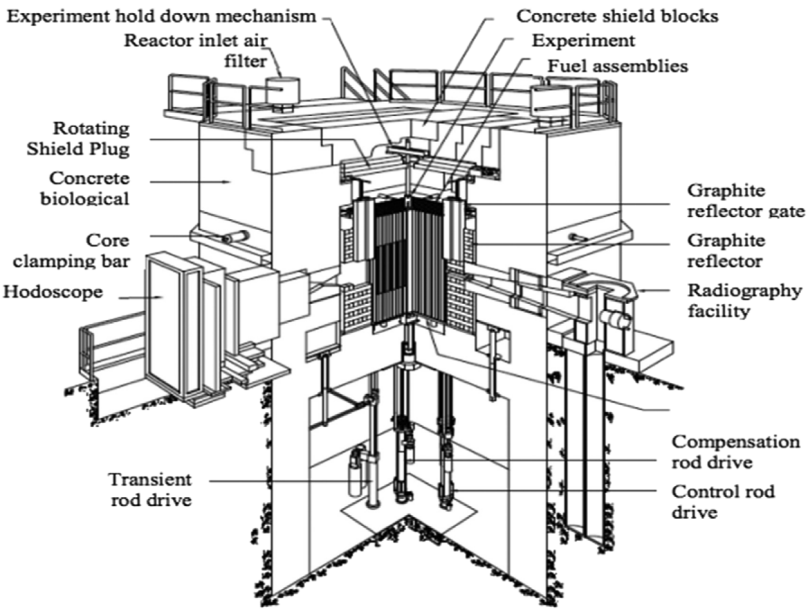

Fig. 1. Schematic of the TREAT facility [2]. Reprinted with license from the publisher.

considered. Fast-sensitive MSNDs are evolutions of well-established thermal-sensitive devices [6]. Recent generations of the MSNDs use ^{6}LiF as the neutron converter. By changing ^{6}LiF to actinide materials and paraffin wax, the actinide and the hydrogenous MSNDs were developed, respectively, to produce fast-neutron sensitive devices.

^{237}Np, ^{235}U, natural uranium, and ^{232}Th were considered for the actinide MSNDs, in which neutrons are converted by fission reaction. Due to the energetic fission fragments, actinide MSNDs allow a high LLD setting to reject neutron-activation gamma rays in the hodoscope. A previous MCNP6 simulation showed the ^{237}Np-filled and the ^{235}U-filled MSNDs yielded efficiencies larger than 1% [7]. In this study, the actinide MSNDs filled with ^{235}U, natural uranium, and ^{232}Th were re-evaluated in Geant4 using the fission fragment generator (FFG) [8]. The FFG samples and tracks fission fragments in a single run to simplify the two-step evaluation in MCNP6 [7]. ^{237}Np-filled MSNDs were not evaluated because Geant4 does not include the neutron data for ^{237}Np [9]. Though absent, the predicted efficiencies of the ^{237}Np-filled MSNDs were better than those of ^{235}U-filled devices [7]. More importantly, ^{237}Np may be preferred to ^{235}U because it is insensitive to neutrons below about 1 MeV, which are generated by the slowing down of the fast neutrons in the test section [3] and the collimator.

The neutron event pulse-height distributions (NEPHDs) of the H-MSNDs were computed in Geant4 and MCNP6 for comparison. The pulse-height distributions (PHDs) of the H-MSNDs from hodoscope-like gamma rays were calculated in Geant4, where the number of source particles per event was adjustable to simulate the gamma ray strength. For completeness, the neutron-detection efficiencies of the H-MSNDs at the 300-keV LLD [10] and the LLD settings that achieved S/N ratio of 100 based on the gamma event PHDs were reported, respectively.

2. Description of the MSND

Shown in Fig. 2 is the basic design of an MSND [11]. The micro-structured trenches are etched into the high-resistivity n-type silicon substrate to a depth of 350 μm [12]. The p-type contacts are diffused along the trenches to form the p–n junction. Then, the trenches are back-filled with neutron converters (historically ^{6}LiF for thermal neutrons). Finally, the ohmic contacts are added.

A neutron entering the detector has a certain possibility to interact with the converters in the trenches and to produce the charge particle(s).

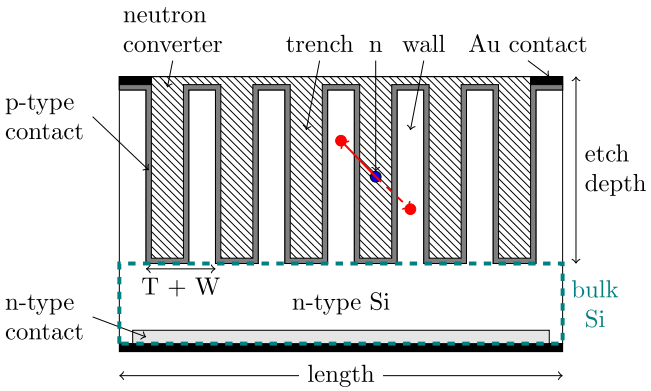

Fig. 2. Basic design of an MSND, where T is the trench width, and W is the wall width.

For the actinide materials, a pair of fission fragments are emitted. For the paraffin wax, a recoil proton is generated. Then, the charge particle(s) might leave the trench and deposit energy in the silicon depletion region. This deposited energy can excite electron–hole pairs. Under applied bias, movement of the charge carriers produces a detectable current. The resulting current can then be amplified, measured, and recorded by the counting electronics [10]. If the resulting current is beyond the LLD setting, a valid count is generated, and the neutron is detected.

A typical ^{6}LiF-filled thermal-sensitive MSND has 20-μm wide trench and 10-μm wall thickness [12]. At a length of 1 cm, it contains approximately 330 trench-wall pairs. A thermal-neutron-sensitive, dual-sided MSND has achieved an intrinsic thermal neutron detection efficiency of approximately 53.54% [12] and a recent upgrade of 69% [13].

3. Cross section comparison of the converters

The fast-sensitive MSND efficiencies depend on the probability that a fast neutron interacts with the converter. Shown in Fig. 3 are the microscopic cross sections of the converting reactions and the neutron spectrum, i.e., the ^{235}U Watt thermal fission spectrum [14], or

$$\chi(E) \propto \exp(-E/0.988)\sinh\left(\sqrt{2.249E}\right). \quad (1)$$

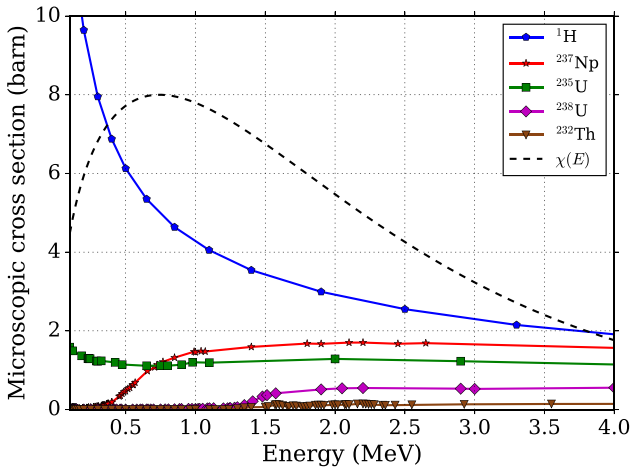

Fig. 3. Microscopic cross sections of the target reactions [15] and the ^{235}U Watt fission spectrum by thermal neutron.

Table 1
Comparison of the converter cross sections.

Converter	Density (g/cm^3)	Molecular weight (g/mole)	$\bar{\sigma}$ (b)	$\bar{\Sigma}$ (cm^{-1})
paraffin wax ($C_{25}H_{52}$ [16])	0.93	352.68	3.93	0.32
^{237}Np	20.25	237.05	1.31	0.067
^{235}U	18.95	235.04	1.21	0.059
^{238}U	18.95	238.05	0.31	0.015
^{232}Th	11.72	232.04	0.075	0.0023

This spectrum peaks at the most-probable neutron energy of approximately 0.74 MeV and leads to an average neutron energy of about 2 MeV.

To quantify the probabilities of the fission neutrons interacting with the nuclides, the fission-spectrum-weighted microscopic cross sections were computed as

$$\bar{\sigma} = \frac{\int_{10^{-11}}^{20\ \mathrm{MeV}} \sigma(E)\chi(E)dE}{\int_{10^{-11}}^{20\ \mathrm{MeV}} \chi(E)dE}, \tag{2}$$

and are shown in Table 1. Paraffin wax has the highest macroscopic cross section of 0.32 cm^{-1}, and ^{237}Np has the largest cross section among actinides by a small margin.

4. Modeling details

4.1. Neutron data library

Performance of fast-sensitive MSNDs was evaluated in Geant4 10.03.p01 [17] and MCNP6.1 [18]. The G4NDL4.5 neutron data library [9] was employed in the Geant4 calculations. This library is primarily based on the ENDF/B-VII.1 nuclear data [15]. Because the G4NDL4.5 library only contains the data for isotopes up to uranium [9], the ^{237}Np-filled MSNDs were not evaluated with Geant4. The MCNP6 calculations used the ENDF/B-VII.0 nuclear data [19]. All cross sections used were for a temperature of 293 K.

4.2. MSND models for NEPHDs

Shown in Figs. 4 and 5 are the MSND models developed for NEPHDs in Geant4 and MCNP6, respectively. Because the neutron-sensitive materials in the MSNDs are primarily the converters in the trenches, these models consisted of the etched silicon region, i.e., the repeated trench-wall structures, as shown in Fig. 6. For illustration, the trench and the wall widths in Figs. 4 and 5 were 0.1 cm. The NEPHDs of the

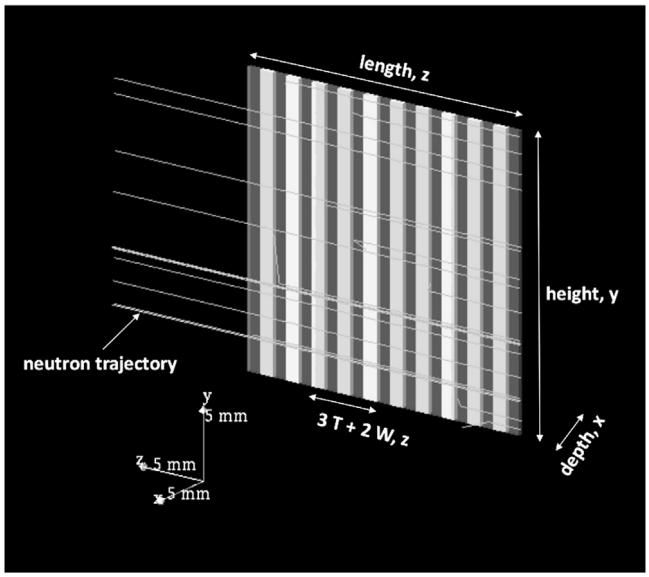

Fig. 4. The developed MSND model for NEPHDs in Geant4. The trench (T) and wall (W) widths were 0.1 cm for illustration.

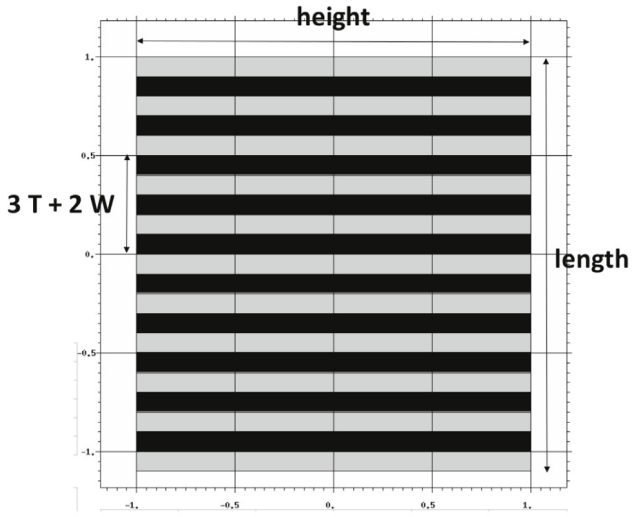

(a) height-length plane

(b) depth-length plane

Fig. 5. The developed MSND model for NEPHDs in MCNP6. The trench (T) and wall (W) widths were 0.1 cm for illustration.

actinide MSNDs were computed in Geant4 using the FFG. The NEPHDs of the H-MSNDs were computed in Geant4 and MCNP6 for comparison.

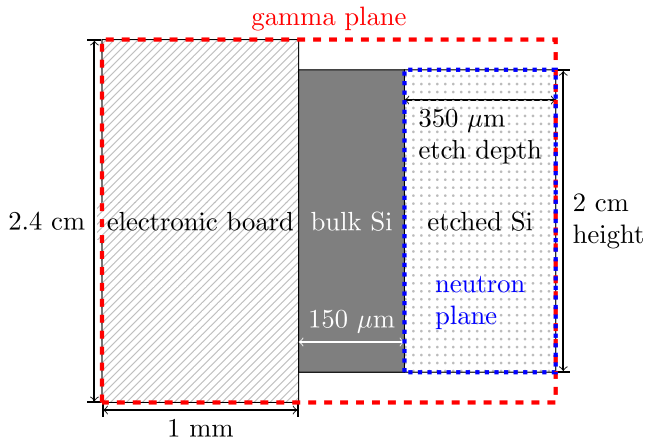

Fig. 6. The etched silicon region was modeled to compute the NEPHDs in Geant4 and MCNP6. To evaluate the H-MSNDs' responses to the gamma rays in Geant4, the bulk silicon region and the electronic board were added. The neutron and the gamma source generation planes were set correspondingly.

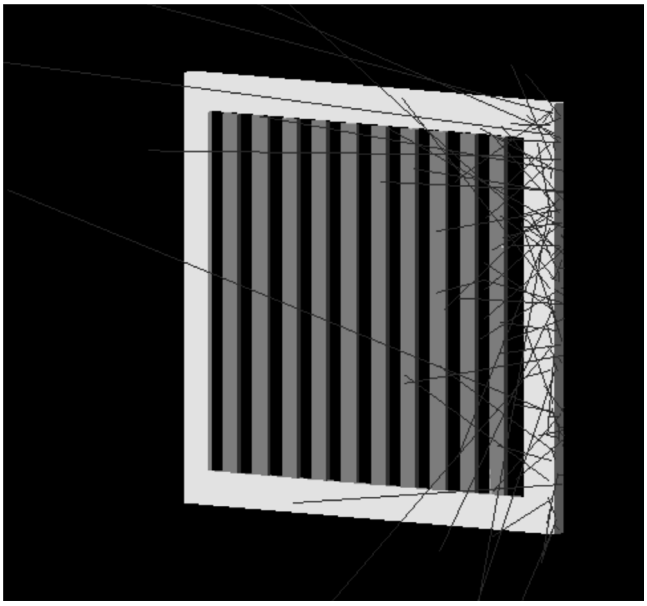

Fig. 7. The H-MSND model to calculate the gamma event PHDs in Geant4.

4.3. MSND model for gamma event PHDs

Shown in Fig. 7 is the H-MSND model to compute the gamma event PHDs in Geant4. In the model, the electronic board, the bulk silicon region, and the etched silicon region were considered. Their dimensions in the height–depth plane are shown in Fig. 6. These volumes were sensitive to the gamma rays due to the relatively high-Z materials. Silicon has an atomic number Z of 14, and the electronic board contained copper ($Z = 29$) and bromine ($Z = 35$).

Geant4 was used to compute the gamma event PHDs because the number of source particles in a pulse event was adjustable [20]. Hence, specific gamma-to-neutron intensity ratio can be sampled to simulate the hodoscope environment.

Based on the Geant4-computed neutron and gamma event PHDs of the H-MSNDs, LLDs that achieved S/N ratio of 100 [21] were set to define the practical neutron-detection efficiencies in the hodoscope. The actinide MSNDs' responses to the gamma rays were not evaluated because the energetic fission fragments allowed high LLD settings intrinsically.

4.4. Physics settings

4.4.1. Geant4 physics setting

The QGSP BERT HP reference physics list [22] was used in the Geant4 calculations. In Geant4, the secondary particle production threshold is specified as the range cut, a distance parameter [20]. Based on the range cut, the production threshold energies for different materials are computed. The energy equivalences of the range cut cannot be lower than a low-edge value, otherwise, the low-edge value will be used. For best accuracy, the low-edge value was set to 250 eV, which is the lower limit for the low-energy electromagnetic processes [17], and the range cut was set to 10 nm to activate the low-edge value. In addition, the produced particles are tracked to zero range [20].

4.4.2. MCNP6 physics setting

In MCNP6, to obtain the most accurate energy deposition, the potential secondary particles (proton, heavy ion, photon, and electron) were transported in the calculations [14]. In the neutron physics card, the analog energy limit parameter, *emcnf*, was set to 100 MeV. This setting performed analog capture for the neutrons with energies smaller than 100 MeV, which provided reliable f8 pulse-height tally. The light-ion and heavy-ion recoil and neutron capture ion algorithm (NCIA) control parameter, *coilf*, was set to the recommended value of four [14], which generated one ion from neutron elastic scattering. In the proton physics card, the *recl* light ion recoil control parameter was set to one. Hence, one light ion was created at each proton elastic scatter event with light nuclei, i.e., hydrogen, deuteron, triton, ^{3}He, and ^{4}He. The default values for the other physics settings were used. The default energy cutoffs for neutron (0), electron (1 keV) and photon (1 keV) were used. The energy cutoffs for the proton and heavy ion were decreased to the lower limit of 1 keV.

4.5. Source terms

4.5.1. Neutron source

In the NEPHD calculations, mono-directional source neutrons traveled along the length-wise direction. The neutron trajectories in Geant4 are shown in Fig. 4. These neutrons were generated uniformly in the depth–height plane of the etched silicon region, as shown in Fig. 6. Energies of the neutrons were sampled from Eq. (1).

4.5.2. Gamma-ray source

Because no detailed neutron-activation gamma-ray information in the hodoscope was reported, several assumptions were made. First, the fission-spectrum gamma rays were used. Second, the gamma rays were emitted into the detector isotropically. Third, the intensity of the gamma rays was 10 per fast neutron.

Because the gamma rays may interact within the electronic board and the silicon substrate, the source gamma rays were born in a plane covering the H-MSND (2.4 cm × 1.5 mm, Fig. 6). Considering the different sampling areas of the neutron and the gamma sources (Fig. 6), to maintain an intensity of 10 gamma rays per fast neutron, the number of gamma rays per event (N_g) was factored to [23]

$$N_g = \frac{A_g}{A_n} \times 10 = \frac{2.4 \times (0.1 + 0.05)}{2 \times 0.035} \times 10 \approx 51, \tag{3}$$

where A_g and A_n are the areas of the gamma-ray and the neutron source planes, respectively.

4.6. Tally methods

In the NEPHD calculations, the deposited energy spectra in the walls were tallied. In the gamma event PHD calculations, the deposited energy spectra in the silicon depletion region, i.e., the walls and the bulk silicon, were tallied.

In Geant4, the deposited energy spectra were computed by the user actions [20]. In MCNP6, the f6 tally by all the tracked particles was first

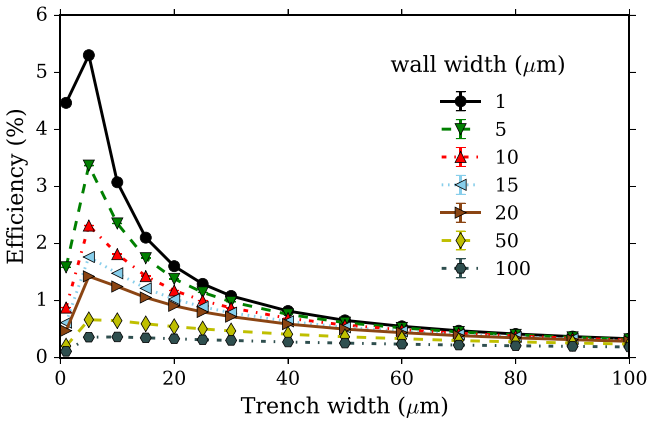

Fig. 8. The Geant4-computed neutron-detection efficiencies of the 2-cm long ^{235}U-filled MSNDs with different trench and wall widths at the 5-MeV LLD.

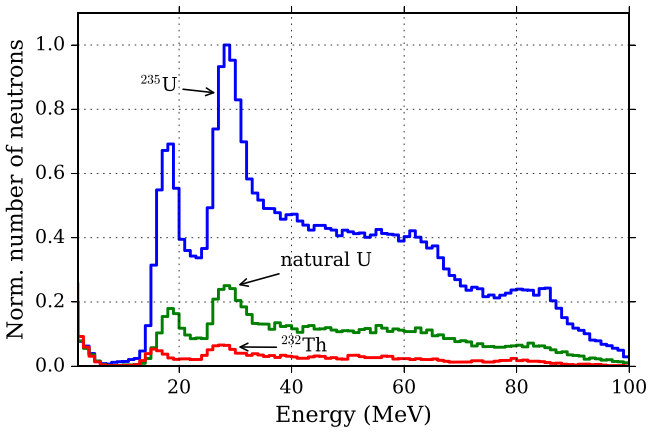

Fig. 9. The Geant4-predicted NEPHDs of the 2-cm long actinide MSNDs with 20-μm trench and 10-μm wall widths.

used to compute the deposited energy in the tally region. Then, based on the f6 tally, the PHD was computed by the *ft phl* option of the f8 tally [14].

4.7. Assumptions of the modeling

To evaluate the MSNDs, a few assumptions were made.

1. The neutron interactions outside the etched silicon region, e.g., the bulk silicon region, were not considered, though these reactions may contribute to the neutron detection efficiency.
2. A perfect charge collection efficiency in silicon was assumed. Indeed, the charge collection efficiency may deteriorate due to the damage or degradation of silicon caused by the fission fragments or protons. These negative effects need further experimental evaluation.
3. The neutrons traveled along the detector length direction perfectly. The impact of any departure from this idealized alignment in practical applications warrants future consideration.

5. Evaluation and results

5.1. Effects of parameters

The fast-sensitive MSNDs with different trench widths, wall widths, and lengths were evaluated. All the detectors had 350-μm depth and 2-cm height. The depth and height were consistent with the current thermal-sensitive MSNDs [12].

For a fixed length, when the trench width is small, an increase of the trench width results in higher neutron-sensitive volume fraction for better efficiency. If the trench width increases further, more charge particles are generated, but a large portion of their energies are deposited in the trenches. Because the electric signal is caused by the energy deposited in the silicon, trapping of the charge particles in the trenches deteriorate the efficiency.

A wider wall enables the charged particles to deposit more energy in the silicon, which allows a higher LLD setting. However, for a fixed length, a wider wall leads to smaller neutron-sensitive volume fraction. Therefore, fewer charged particles are generated. Additionally, a wider wall increases the H-MSND's gamma sensitivity.

For fixed trench and wall widths, a longer MSND yields better efficiency because the neutron penetrates more trench-wall pairs. Longer lengths can be achieved by stacking the processed silicon substrates into an array, similar to proposed ^{3}He replacement devices [24]. The length is also limited by the space in the hodoscope to install the MSND, i.e., approximately 20 cm.

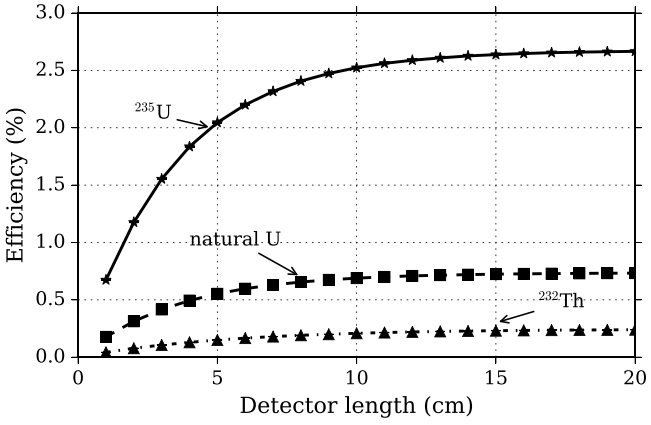

Fig. 10. The Geant4-computed intrinsic neutron detection efficiencies of the actinide MSND arrays. The MSNDs had 20 μm trench and 10 μm wall widths. The LLDs were set to 5 MeV.

5.2. Actinide MSNDs

5.2.1. Trench-wall optimization

Shown in Fig. 8 are the Geant4-computed neutron detection efficiencies of the 2-cm long ^{235}U-filled MSNDs with different trench and wall widths at a LLD setting of 5 MeV. With 20-μm trench and 10-μm wall widths, the ^{235}U-filled MSND yields intrinsic neutron detection efficiency of about 1.2%. Though better efficiencies are achievable with smaller trench widths, filling the trenches with uranium has proven difficult [7].

5.2.2. NEPHDs

NEPHDs of the actinide MSNDs with 2-cm length, 20-μm trench and 10-μm wall widths are shown in Fig. 9. These PHDs feature two peaks at about 18 MeV and 30 MeV, respectively. The PHDs indicate the actinide MSNDs allow high LLD settings, e.g., 10 MeV.

5.2.3. Efficiencies of the actinide MSND arrays

With 20-μm trench and 10-μm wall widths, intrinsic neutron detection efficiencies of the actinide MSNDs with different lengths are shown in Fig. 10. The 5-MeV LLD was applied. The ^{235}U-filled MSNDs with lengths larger than 14 cm yield intrinsic neutron detection efficiency of about 2.6%. The MSNDs filled with natural uranium and ^{232}Th cannot achieve efficiencies larger than 1%.

Table 2
Total deposited energies (MeV) in the trenches per neutron computed by Geant4 and MCNP6 and their differences (relative to MCNP6).

	MCNP6	Geant4	Difference (%)
^{235}U	10.44 ± 0.19%	10.37 ± 0.39%	−0.70 ± 0.43
Natural Uranium	2.75 ± 0.44%	2.64 ± 0.80%	−4.07 ± 0.87
^{232}Th	0.46 ± 0.48%	0.42 ± 1.89%	−6.84 ± 1.82

Table 3
Alpha decays of the 2-cm long actinide MSNDs with 20-μm trench and 10-μm wall widths.
Source: Data from Ref. [25].

Reactant	Half life (s)	Number of α particles in 10 μs	Most-probable α energy (MeV) (abs. %)
^{235}U	2.22×10^{16}	1.41	4.40 (57.73)
^{238}U	1.41×10^{17}	0.22	4.20 (79.00)
^{232}Th	4.42×10^{17}	0.045	4.01 (78.20)

5.2.4. Comparison between Geant4 and MCNP6

The Geant4-computed and the MCNP6-computed total deposited energies in the trenches per neutron of the actinide MSNDs were compared. The MSNDs had the geometry of 2-cm length, 20-μm trench, and 10-μm wall widths (orientation of the dimensions is shown in Fig. 2). This particular comparison was made because MCNP6 assumes the fission energy is deposited locally [14]. To be consistent, the FFG in Geant4 was turned off.

Shown in Table 2 are the computed results, which agree relatively well. For ^{235}U, the Geant4-computed tally differs from the MCNP6 value by about −0.7%. The differences might be caused by the different cross section libraries used by the two codes, as discussed in Section 4.1.

5.2.5. Alpha decay of the reactants

Besides the necessity of discriminating gamma rays in the hodoscope environment, the LLD of the actinide MSNDs must be set to account for the decay alpha particles of the converters. Table 3 summarizes the alpha decay information of the actinide reactants in the MSNDs with the geometry of 2-cm length, 20-μm trench, and 10-μm wall widths. The energies of the alpha particles are approximately 4 MeV. In the 10-μs pulse shaping time of current MSND [10], the number of alpha particles would not exceed 1.41. Hence, a 5-MeV LLD should be sufficient to reject the alpha particles and the gamma rays. In addition, based on the NEPHDs (Fig. 9), the LLD can be set to 10 MeV without significant efficiency deterioration.

5.3. Hydrogenous MSNDs

5.3.1. Trench-wall optimization at 300-keV LLD

At 300-keV LLD, the intrinsic neutron detection efficiencies of the 2-cm long H-MSNDs with different trench and wall widths were computed in Geant4 and MCNP6, and the results are shown in 11. Results of the two codes agree well, and the slight differences may be caused by the different cross-section libraries (Section 4.1). With 20-μm trench and 10-μm wall widths, the efficiency of about 10% was predicted.

5.3.2. NEPHDs at 300-keV LLD

Shown in Fig. 12 are the Geant4- and MCNP6-computed NEPHDs of the 2-cm H-MSND with 20-μm trench and 10-μm wall widths. A peak at about 500 keV exists.

5.3.3. Efficiencies of the H-MSND array at 300-keV LLD

With 20-μm trench and 10-μm wall widths, the Geant4- and MCNP-computed intrinsic neutron detection efficiencies of the H-MSNDs with different lengths are shown in Fig. 13. A 300-keV LLD was applied. The efficiency saturates at about 26%.

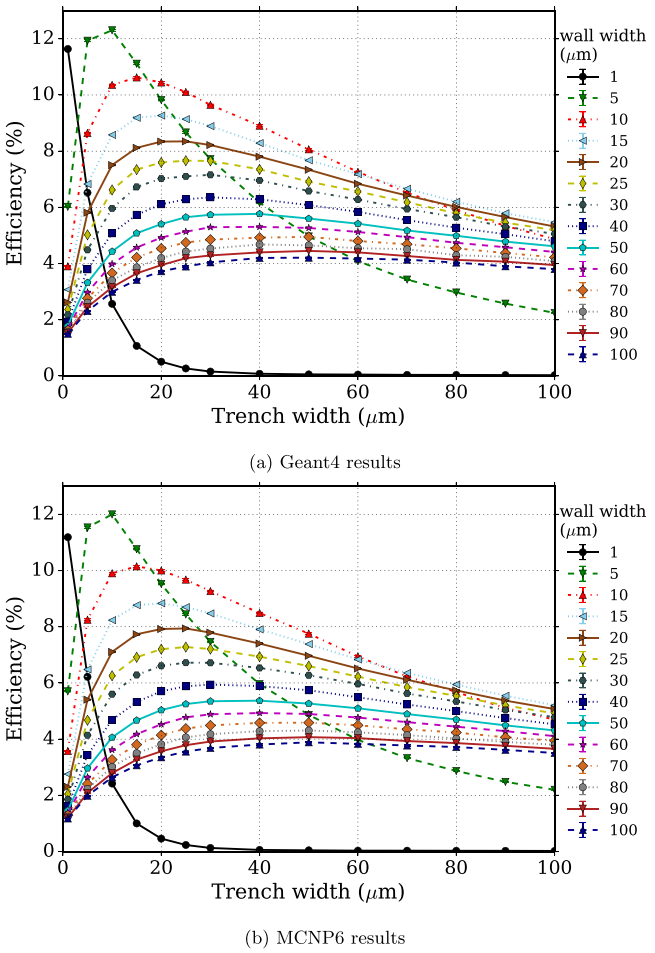

Fig. 11. The Geant4- and MCNP6-computed intrinsic neutron detection efficiencies of the 2-cm long H-MSNDs with different trench and wall widths. A 300-keV LLD was set.

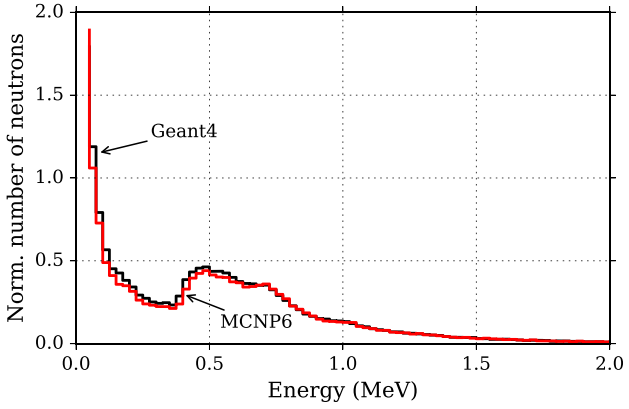

Fig. 12. The Geant4- and MCNP6-computed NEPHDs of the 2-cm long H-MSND with 20-μm trench, 10-μm wall widths.

5.3.4. Trench-wall optimization at S/N 100

Table 4 summarizes the trench and wall widths of the 2-cm long H-MSNDs that yielded intrinsic neutron detection efficiencies larger than 2% . The LLDs were set to achieve an S/N ratio of 100 based on the neutron and the gamma event PHDs computed by Geant4. The H-MSND with 60-μm trench and 40-μm wall widths yields the best efficiency of 2.47%, where the 1.2-MeV LLD is set to achieve an S/N ratio of 100.

Table 4
The trench and wall widths of the 2-cm long H-MSNDs that yielded neutron detection efficiencies (in percent) above 2% at the LLD settings that achieved S/N ratio of 100. The LLD settings in MeV are shown in the parentheses.

Trench (μm)	Wall (μm)				
	25	30	40	50	60
40	2.01 (1.225)	2.21 (1.250)	2.21 (1.325)		
50		2.37 (1.175)	2.20 (1.300)	2.15 (1.350)	
60	2.04 (1.125)	2.28 (1.150)	**2.47 (1.200)**	2.29 (1.275)	2.04 (1.350)
70		2.35 (1.100)	2.41 (1.175)	2.25 (1.250)	2.11 (1.300)
80		2.18 (1.100)	2.36 (1.150)	2.32 (1.200)	2.09 (1.275)
90			2.30 (1.125)	2.20 (1.200)	2.11 (1.250)
100			2.18 (1.125)	2.15 (1.200)	2.14 (1.200)

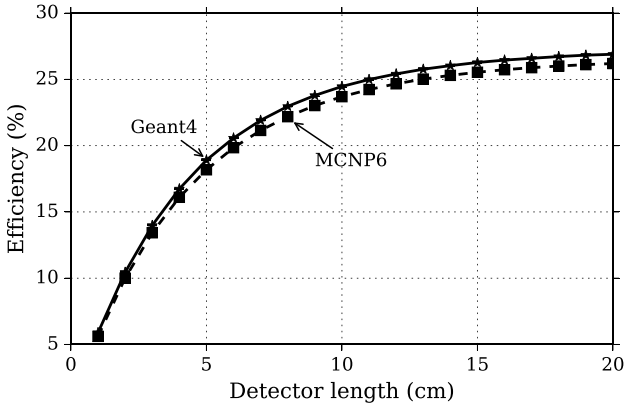

Fig. 13. The Geant4- and MCNP6-computed neutron detection efficiencies of the H-MSNDs with different lengths. The 300-keV LLD was set. The H-MSNDs were with 20-μm trench and 10-μm wall widths.

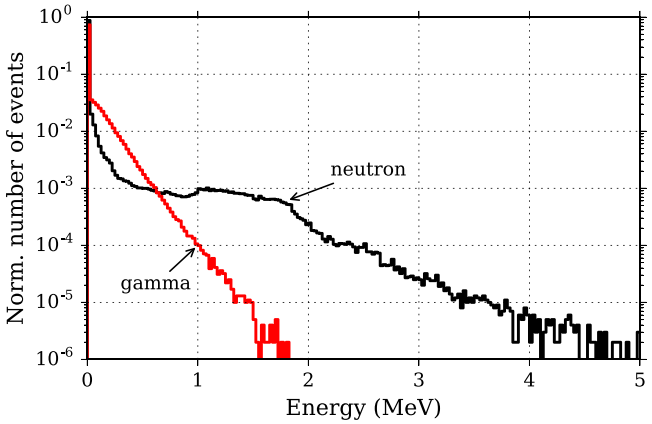

Fig. 14. The Geant4-computed neutron and gamma event PHDs of the 2-cm long H-MSND with 60-μm trench and 40-μm wall widths.

5.3.5. *Neutron and gamma event PHDs at S/N 100*

Fig. 14 shows the Geant4-computed neutron and gamma event PHDs of the 2-cm long H-MSND with the optimized 60-μm trench and 40-μm wall widths. The peak of the NEPHD is beyond 1 MeV.

5.3.6. *Efficiencies of the H-MSND array at S/N 100*

With 60-μm trench and 40-μm wall widths, the neutron-detection efficiencies of the H-MSNDs with different lengths are shown in Fig. 15. The LLDs were set to achieve S/N ratio of 100. The maximum efficiency of about 9.6% is predicted at the length of 20 cm.

6. Conclusion

Performance of the actinide MSNDs and the H-MSNDs for the TREAT hodoscope was evaluated in Geant4 and MCNP6. The actinide MSNDs

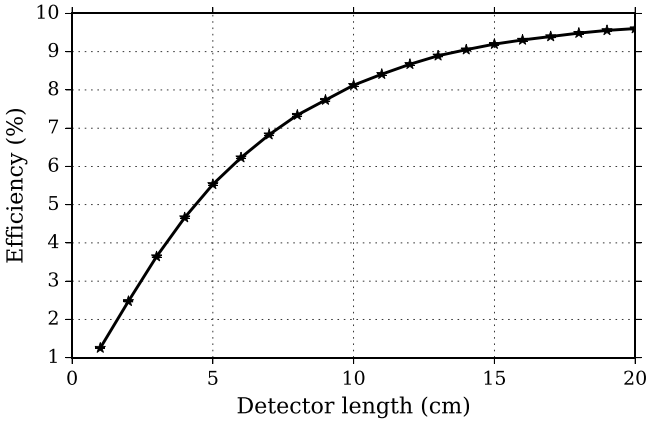

Fig. 15. The Geant4-computed neutron detection efficiencies of the H-MSNDs vary with length. The H-MSNDs had the optimized 60-μm trench and 40-μm wall widths. The LLDs were set to achieve an S/N ratio of 100 based on the gamma event PHDs.

allow high LLD settings due to the energetic fission fragments, while paraffin wax in the H-MSNDs leads to more fast neutron interactions. The actinide MSNDs filled with ^{235}U, natural uranium, and ^{232}Th were evaluated using the FFG in Geant4. Applying a 5-MeV LLD to reject the gamma rays and decay alpha particles, the 2-cm ^{235}U-filled MSND with 20-μm trench and 10-μm wall widths yielded intrinsic neutron detection efficiency of about 1.2%. For this MSND, the Geant4 computed deposited energy in the trenches differed from the MCNP6 result by about −0.7%. With these trench and wall widths, the efficiency of the ^{235}U-filled MSND array saturated at about 2.6%, where a 5-MeV LLD was set. The efficiencies of the ^{235}U-filled MSNDs acted as the lower limits of the ^{235}Np-filled devices, which are preferred due to their insensitivity to the slow neutrons. The MSNDs filled with natural uranium and thorium were predicted to have efficiencies lower than the 1% target.

The NEPHDs of the H-MSNDs computed by Geant4 and MCNP6 agreed relatively well. At 300-keV LLD, the 2-cm long H-MSND with 20-μm trench and 10-μm wall widths yielded intrinsic neutron detection efficiency of about 10%. With these trench and wall widths, the 20-cm long H-MSND yielded an efficiency of about 26% at a 300-keV LLD.

The H-MSNDs' responses to the hodoscope-like gamma rays were computed in Geant4. Based on the Geant4-computed neutron and gamma event PHDs, the LLDs were set to achieve S/N ratio of 100, and the 2-cm long H-MSND yielded the best neutron detection efficiency of about 2.47% with the 60-μm trench and 40-μm wall widths. Setting the LLD in the same way, the H-MSND array with the optimized trench and wall widths yielded a neutron detection efficiency of about 9.6% at a length of 20 cm.

The MSNDs in this paper were with 350-μm depth and 2-cm height. The cross section of a slit in the hodoscope collimator is $\frac{1}{16} \times \frac{3}{16}$ inch (1.6×4.8 mm) [3]. To fit the slit, several MSNDs may be stacked, which will be investigated in further iterations.

As a final note, the results in this paper are entirely computational in nature. Though promising, the designs explored and results reported should be validated experimentally. Preliminary work has been performed to test H-MSNDs in the piercing beam of the KSU TRIGA Mark II [26]. However, the beam is not sufficiently characterized and known to be dominated by sub-fast neutron and gamma-ray signals. Some work has been performed to characterize the beam with and without filters that reduce these undesirable signals [27]. When complete, the filtered beam will be better suited for testing of fast-sensitivity devices like those presented here.

Acknowledgments

The material presented is based upon work supported by the U.S. Department of Energy, Office of Nuclear Energy under Award Number DE-NE0008305. Some of the computing for this study was performed on the Beocat Research Cluster at Kansas State University, which is funded in part by NSF (National Science Foundation) grants CNS-1006860, EPS-1006860, and EPS-0919443.

References

[1] M.D. DeHart, B.A. Baker, J. Ortensi, Interpretation of energy deposition data from historical operation of the transient test facility (TREAT), Nucl. Eng. Des. 322 (2017) 504–521.
[2] D.D. Imholte, F. Aydogan, Comparison of nuclear pulse reactor facilities with reactivity-initiated-accident testing capability, Prog. Nucl. Energy 91 (2016) 310–324.
[3] A.D. Volpi, R. Pecina, R. Daly, D. Travis, R. Stewart, E. Rhodes, Fast-neutron hodoscope at TREAT: development and operation, Nucl. Technol. 27 (3) (1975) 449–487.
[4] V.K. Patel, M.A. Reichenberger, J.A. Roberts, T.C. Unruh, D.S. McGregor, MCNP6 simulated performance of Micro-Pocket Fission Detectors (MPFDs) in the Transient REActor Test (TREAT) facility, Ann. Nucl. Energy 104 (2017) 191–196.
[5] J.K. Shultis, R.E. Faw, Fundamentals of Nuclear Science and Engineering, third ed, CRC press, 2016.
[6] S.L. Bellinger, R.G. Fronk, T.J. Sobering, D.S. McGregor, High-efficiency microstructured semiconductor neutron detectors that are arrayed, dual-integrated, and stacked, Appl. Radiat. Isot. 70 (7) (2012) 1121–1124.
[7] P. Ghosh, W. Fu, R. Fronk, D.S. McGregor, J.A. Roberts, Evaluation of MSNDs for fast-neutron detection and the TREAT hodoscope, Trans. Am. Nucl. Soc. 115 (2016) 1009–1012.
[8] J. Allison, K. Amako, J. Apostolakis, et al., Recent developments in Geant4, Nucl. Instrum. Methods Phys. Res. A 835 (2016) 186–225.
[9] T. Koi, D.H. Wright, L. Desorgher, Simulation of the production of radionuclides using Geant4, https://public.ornl.gov/neutrons/conf/aria2015/presentations/04%20Simulation%20of%20the%20Production%20of%20Radionuclides%20Using%20Geant4.pdf.
[10] R.G. Fronk, S.L. Bellinger, L.C. Henson, T.R. Ochs, C.T. Smith, J.K. Shultis, D.S. McGregor, Dual-sided microstructured semiconductor neutron detectors (DSMSNDs), Nucl. Instrum. Methods Phys. Res. A 804 (2015) 201–206.
[11] D. McGregor, S. Bellinger, R. Fronk, L. Henson, D. Huddleston, T. Ochs, J. Shultis, T. Sobering, R. Taylor, Development of compact high efficiency microstructured semiconductor neutron detectors, Radiat. Phys. Chem. 116 (2015) 32–37.
[12] R.G. Fronk, S.L. Bellinger, L.C. Henson, et al., Advancements on dual-sided microstructured semiconductor neutron detectors (DSMSNDs), in: Proc. IEEE Nucl. Sci. Symp. Med. Imag. Conf. (NSS/MIC), 2015, pp. 1–4.
[13] T. Ochs, S. Bellinger, R. Fronk, L. Henson, R. Hutchins, D. McGregor, Improved manufacturing and performance of the dual-sided microstructured semiconductor neutron detector, Nucl. Instrum. Methods Phys. Res. A (2018) submitted for publication.
[14] D. Pelowitz, T. Goorley, M. James, et al., MCNP6 User's Manual, version 1.0, 2013.
[15] M. Chadwick, M. Herman, P. Obložinskỳ, M.E. Dunn, Y. Danon, A. Kahler, D.L. Smith, B. Pritychenko, G. Arbanas, R. Arcilla, et al., ENDF/B-VII.1 nuclear data for science and technology: cross sections, covariances, fission product yields and decay data, Nucl. Data Sheets 112 (12) (2011) 2887–2996.
[16] R.J. McConn, C.J. Gesh, R.T. Pagh, R.A. Rucker, R. Williams III, Compendium of material composition data for radiation transport modeling, Tech. rep., Pacific Northwest National Laboratory (PNNL), Richland, WA (US), 2011.
[17] S. Agostinelli, J. Allison, K.a. Amako, J. Apostolakis, H. Araujo, P. Arce, M. Asai, D. Axen, S. Banerjee, G. Barrand, et al., GEANT4-a simulation toolkit, Nucl. Instrum. Methods Phys. Res. A 506 (3) (2003) 250–303.
[18] T. Goorley, M. James, T. Booth, F. Brown, J. Bull, L. Cox, J. Durkee, J. Elson, M. Fensin, R. Forster, et al., Initial MCNP6 release overview, Nucl. Technol. 180 (3) (2012) 298–315.
[19] M. Chadwick, P. Obložinskỳ, M. Herman, N. Greene, R. McKnight, D. Smith, P. Young, R. MacFarlane, G. Hale, S. Frankle, et al., ENDF/B-VII.0: next generation evaluated nuclear data library for nuclear science and technology, Nucl. Data Sheets 107 (12) (2006) 2931–3060.
[20] Geant4 collaboration, Geant4 user's guide for application developers, Geant4 10.3 Edition, 2016.
[21] H.J.M. Chichester, Advanced fuels campaign in-reactor instrumentation overview, https://www.energy.gov/sites/prod/files/2015/11/f27/7.%20Advanced%20Fuels%20Program%20In-Reactor%20Instrumentation%20Overview.pdf, 2015.
[22] Reference physics lists, http://geant4.cern.ch/support/proc_mod_catalog/physics_lists/referencePL.shtml.
[23] W. Fu, P. Ghosh, M.J. Harrison, D.S. McGregor, J.A. Roberts, A Geant4 evaluation of the Hornyak button and two candidate detectors for the TREAT hodoscope, Nucl. Instrum. Methods Phys. Res. A 889 (2018) 39–46.
[24] T.R. Ochs, S.L. Bellinger, R.G. Fronk, L.C. Henson, D.E. Huddleston, Z.I. Lyric, J.K. Shultis, C.T. Smith, T.J. Sobering, D.S. McGregor, Present status of the microstructured semiconductor neutron detector (MSND)-based direct helium-3 replacement, IEEE Trans. Nucl. Sci. (2017).
[25] Live chart of nuclides, nuclear structure and decay data, https://www-nds.iaea.org/relnsd/vcharthtml/VChartHTML.html.
[26] J.A. Roberts, M.J. Harrison, W. Fu, P. Ghosh, D.S. McGregor, Fast-neutron detector developments for the treat hodoscope, Radiat. Phys. Chem. (2018) http://dx.doi.org/10.1016/j.radphyschem.2018.06.008.
[27] J.C. Boyington, R.L. Reed, R.M. Ullrich, J.A. Roberts, Gamma-ray and thermal-neutron filter design for a TRIGA penetrating beam port, Trans. Am. Nucl. Soc. 117 (2017) 1162–1165.